Protein conformational space at the edge of allostery: turning a nonallosteric malate dehydrogenase into an "allosterized" enzyme using evolution-guided punctual mutations

Antonio Iorio, Céline Brochier-Armanet, Caroline Mas, Fabio Sterpone, Dominique Madern

Protein Conformational Space at the Edge of Allostery: Turning a Non-allosteric Malate Dehydrogenase into an "Allosterized" Enzyme using Evolution Guided Punctual Mutations

Antonio Iorio[1], Céline Brochier-Armanet[2], Caroline Mas[3] Fabio Sterpone[1]* and Dominique Madern[3]*

1- CNRS, Université de Paris, UPR 9080, Laboratoire de Biochimie Théorique, Paris, France; Institut de Biologie Physico-Chimique-Fondation Edmond de Rothschild, PSL Research University, Paris, France.

2- Univ Lyon, Université Lyon 1, CNRS, UMR5558, Laboratoire de Biométrie et Biologie Évolutive, 43 bd du 11 novembre 1918, F-69622, Villeurbanne, France.

3-Univ. Grenoble Alpes, CEA, CNRS, IBS, 38000 Grenoble, France

* Corresponding authors:

Dr Dominique Madern, Dr Fabio Sterpone,

Abstract.

We unveil the intimate relationship between protein dynamics and allostery by following the trajectories of model proteins in their conformational and sequence spaces. Starting from a non-allosteric hyperthermophilic malate dehydrogenase, we have tracked the role of protein dynamics in the evolution of the allosteric capacity. Based on a large phylogenetic analysis of the malate (MalDH) and lactate dehydrogenase (LDH) superfamily, we identified two amino acid positions that could have had a major role for the emergence of allostery in LDHs, which we targeted for investigation by site-directed mutagenesis. Wild type MalDH and the single and double mutants were tested with respect to their substrate recognition profiles. The double mutant displayed a sigmoid shaped profile typical of homotropic activation in LDH. By using molecular dynamics simulations, we showed that the mutations induce a drastic change in the protein sampling of its conformational landscape, making transiently T-like (inactive) conformers, typical of allosteric LDHs, accessible. Our data fit well with the seminal key concept linking protein dynamics and evolvability. We showed that the selection of a new phenotype can be achieved by a few key dynamics-enhancing mutations causing the enrichment of low populated conformational sub-states.

Introduction.

Allostery is the process in which protein catalytic efficiency is regulated by the binding of an effector at a specific distal site from the catalytic site (Wodak et al. 2019). According to initial models of allostery, the process relies on a ligand-dependent conformational change between a tense inactive state (T-state) and a relaxed active state (R-state) (Monod et al.1965; Koshland et al.1966). Later, extensive analyses have shown that allosteric regulation is grounded in the protein dynamics, leading tothe unifying and general "ensemble model" of allostery (Hisler et al. 2012; Motlagh et al. 2014; Biddle et al. 2021). In this model, the allosteric capacity of an enzyme depends on the reorganization of the protein conformational landscape, induced by events such as interactions with others protein partners or ligands, local unfolding, and physicochemical variations of the environment (Schrank et al. 2009; Arai et al. 2010; Lisi et al. 2018; Halgand et al. 2020; Iorio et al. 2021).

Protein superfamilies encompassing allosteric and non-allosteric enzymes are under study to disclose the molecular mechanisms of allosteric regulation (Huang et al., 2014; Suplatov and Svedas, 2015). Indeed, deciphering the evolutionary history of these super families can enhance our understanding of the structure, function, and dynamical relationships that allowed allostery to emerge (reviewed in Modi et al. 2021).Here we focus on the lactate/malate dehydrogenase (LDH / MalDH) superfamily. LDH (EC 1.1.1.27) are 2-ketoacid: NAD(P)-dependent dehydrogenases that catalyze the reversible conversion of 2-hydroxyacids to the corresponding 2-ketoacids. LDHs are involved in energy metabolism and operate at the final stage of glycolysis (Holbrook et al. 1975; Ferst 1985; Adeva-Andany et al. 2014). They reversibly transform pyruvate (PYR) into lactate using NADH as coenzyme. Most bacterial LDHs are allosterically regulated, i.e., they display sigmoid kinetics as a function of PYR concentration (homotropic activation) and are activated in the presence of the allosteric effector fructose 1,6-bisphosphate (FBP) (heterotropic activation) (Garvie1980; Schroeder et al. 1988; Arai et al. 2002; Feldman-Salit et al. 2013; Taguchi.2017). In contrast, LDHs from eukaryotes are thought as non-allosteric, a consideration mainly based on the characterization of vertebrates enzymes, even if this has been recently challenged (Iacovino et al 2022).

The catalytic mechanism of LDH has been studied extensively. In its competent catalytic state, LDH catalyzes the direct transfer of a hydride ion from the pro-R face of NADH to the C2 carbon of PYR to produce lactate. The complete process involves a set of several amino acids, with specific roles (Burgner et al. 1984; Clarke et al. 1986; Clarke et al. 1988; Deng et al. 1994; McClendon et al. 2005; Deng et al. 2011). The amino acids, listed according to the LDH

nomenclature (Eventoff et al. 1977), are: the reactive histidine H195, glutamic acid D168 that helps to polarize H195, arginine R109 that stabilizes the transition state, the substrate binding residue arginine R171, and glutamine Q102 that sustains specifically the recognition of the PYR. In the catalytic site, threonine T246, which is conserved in all LDH sequences, also contributes to the correct geometry and favorable chemistry, ensuring efficient catalysis (Bur et al. 1989, Sakiwicz et al. 1993*)*. In LDHs, there is always an acid residue (D or E) at position 199, which contributes to charge neutrality when the mobile loop covers the catalytic site (Wilks et al. 1988).

The crystal structures of allosteric LDHs without (Apo) and with ligands (Holo) revealed large conformational changes that are representative of the transition between the T- and R-states (Piontek et al. 1990; Wigley et al. 1992; Iwata et al. 1994; Auerbach et al. 1998; Winter et al. 2003; Coquelle et al. 2007; Arai et al. 2010; Colletier et al. 2012; Matoba et al. 2014; Kolappan et al. 2015). These structural reorganizations involve changes such as the expansion or compaction of the quaternary scaffold together with some helix sliding and local rearrangements within the catalytic site (see the review by Taguchi 2017). In structures typical of the R-active state, a mobile loop that carries the substrate discriminating glutamine Q102 covers the catalytic site, allowing its dehydration and the correct anchoring of PYR with the side chain of R171, which protrudes within the catalytic site. In contrast, representative structures of the T-inactive state, show that the R171 side chain is outside the catalytic site, demonstrating that its position is a strong proxy of allosteric capacity (Colletier et al. 2012; Iorio et al. 2021). Furthermore, in allosteric LDHs, H68 and R171 are close to each other with coordinated side chain conformations. In Apo structures of LDHs, H68 is in a conformation that hinders the entry of the side chain of R171 into the catalytic site.

In addition to LDHs, the LDH/MalDH superfamily includes also malate dehydrogenases (MalDH, EC 1.1.1.37) and hydroxyisocaproate dehydrogenases (HicDH) (Madern 2002; Madern et al. 2004; Boucher et al. 2014). MalDHs are involved in the tricarboxylic acid cycle (TCA) and oxidize oxaloacetate (OAA) into malate using NAD(P)Has coenzyme (Minárik et al. 2002).Despite a similar catalytic mechanism and common structural scaffold, the substrate recognition mechanism between LDHs and MalDHs is very stringent. This discriminating effect relies mainly on the nature of the amino acid at position 102, which is Q102 in LDHs and R102 in MalDHs (Wilks et al. 1998; Chapman et al. 1999). MalDHs have been divided into three subgroups: the dimeric MalDH type 1 and MalDH type 2, and the tetrameric MalDH type 3. Phylogenetic analyses showed that at least four MalDH toward LDH functionality occurred. More precisely, canonical LDH, LDH of *Plasmodium*- and *Cryptosporidium*-related species

derived independently from ancient MalDH type 3, while the LDH of *Trichomonas vaginalis* derived from MalDH type 1 (Madern 2002; Zhu and Keithly 2002; Madern et al. 2004; Boucher et al. 2014; Steindel et al 2016;Brochier-Armanet and Madern 2021). Regarding canonical LDH, the transition occurred from within an intermediate group of sequences with various affinities and substrate discrimination capacities, which can be considered as a reservoir of enzymes prone to evolve new phenotypes (Brochier-Armanet and Madern 2021).Sequences of this intermediate group branch in-between MalDH type 3 and LDH. They form several subgroups (referred as to A to P) and harbor variable combinations of amino acids that are usually specific of either LDH (Q102, D/E199, and T246) or MalDH type 3 (R102, M199, and A/S246). The LDH capacity to recognize and use PYR as substrate, was in part the consequence of the acquisition of a permissive amino acid, a threonine (T) at amino acid position 246, early during the diversification of the intermediate group of MalDH (Brochier-Armanet and Madern 2021). T246 is also considered as unfavorable for OAA binding (Bur et al. 1989). Strengthening this proposal, some MalDHs of the intermediate group that harbors T246 recognize both OAA and PYR as substrates (Roche et al., 2019). Later, the fixation of a glutamine (Q) in position 102 granted binding specificity toward PYR (Brochier-Armanet and Madern 2021). This substitution occurred in the stem of the canonical LDH clade.

Studying enzymes from the intermediate group could provide useful information to describe how allosteric properties evolved within the MalDH/LDH super family. Until now, no allosteric behavior has been reported for MalDHs type3, whereas some MalDHs from the intermediate groups of sequences displayed a latent (i.e. hidden) allosteric capacity, underpinning their close relationship with LDHs (Roche et al. 2019; Katava et al. 2020; Brochier-Armanet and Madern, 2021). Note that the complete allosteric regulation via homotropic and heterotropic activation, as in the case of canonical allosteric LDHs, has not been reported in any enzyme of the MalDH intermediate group.

In this study, by comparing structures, we identified a combination of three critical amino acids (at position 68, 102 and 250) that could be related to the emergence of allosteric capacity from MalDHs to LDHs and we showed that the nature of amino acid at position 250 plays a major role for the selection of allosteric capacity in LDH. This hypothesis was then addressed by using site-directed mutagenesis on the enzyme of *Archaeoglobus fulgidus (A. ful)*, a dimeric MalDH belonging to the intermediate group that has been characterized biochemically and structurally (Madern et al. 2001; Irimia et al. 2004). The replacement ofP250 by an isoleucine in conjunction with the replacement of the R102 by Q102 revealed important changes in dynamical properties that allowed the non-allosteric *A. ful* MalDH to turn into a

homotropically activated dimeric LDH. Our study strongly suggests that the allosteric properties in LDHs emerged from non-allosteric MalDHs, via an intermediate group of enzymes, in which a few key mutations induced a reorganization of their conformational landscape rendering them prone to evolve allosteric regulation.

Results

Investigating the phylogeny of the LDH / MalDH superfamily suggests that the universal conserved position I250 could be a key determinant for allostery

We used the recently published LDH / MalDH phylogeny (Brochier-Armanet and Madern 2021) to reveal candidate amino acids that could be linked to allosteric behavior. More precisely, we focused on the large clade encompassing the LDHs, the MalDH type 3, and the intermediate group that branches in-between LDHs and MalDH type 3. The intermediate group displayed enzymes with mixed properties with respect to substrate recognition (Brochier-Armanet and Madern 2021). Based on structural and sequence comparisons, we explored the organization of the catalytic site of LDH, MalDH type 3, and the intermediate group of MalDH (fig. 1*a*, *b*, *c* and *d*).

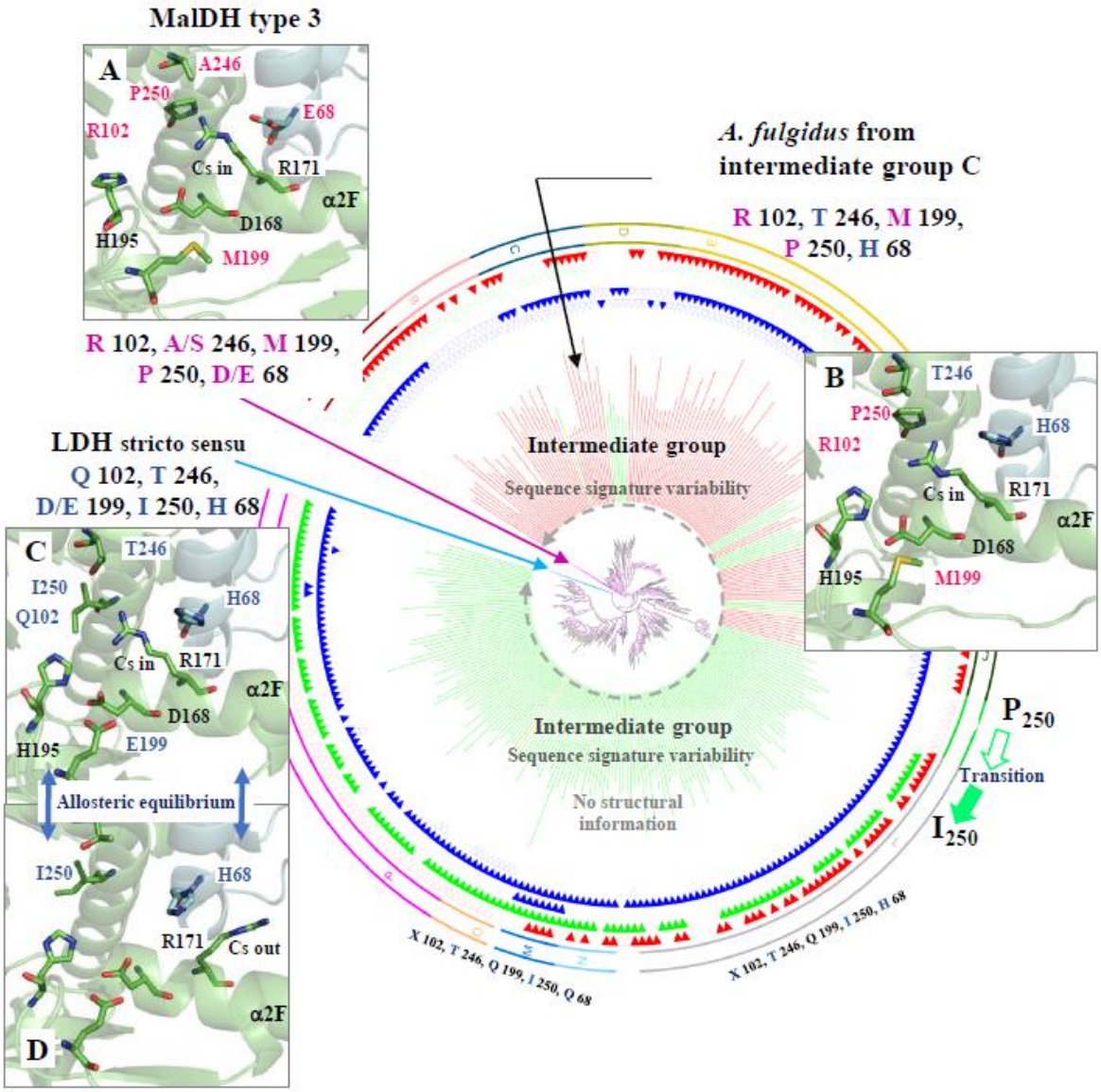

FIG. 1. Unrooted maximum likelihood phylogeny of the LDHs, MalDH type 3, and intermediate MDHs. An extended view of the tree is presented in Supplementary Figure S1. The blue and purples branches correspond to LDHs and MalDH type 3 (for clarity the corresponding clades have been collapsed and are indicated by arrows). Branches of the intermediate group of MalDH are coloured according to the taxonomy: green indicates bacterial sequences, red archaeal sequences, and yellow eukaryotic sequences. Sequences of the MalDH intermediate group display mixed combinations of the LDH and MalDH type signatures. The circular regions made of triangles correspond to critical residues: Empty triangles correspond to residues usually found in MalDH type 3, while filled residues are similar to those found in LDHs. More precisely, the most inner circle corresponds to Q102 (filled blue triangles), R102 (empty triangles), or other residues (no triangle), the second circle to T246 (filled blue triangles), A/S246 (empty blue triangles), or other residues (no triangle), the filled triangles on third circle design an acidic residue (D/E199) that ensure charge neutrality within the catalytic site of LDH, the fourth circle to I250 (filled green triangles), P250 (empty green triangles), or other residues (no triangle), and the fifth circle to H68 (filled red triangles), D/Q68 (empty triangles), or other residues (no triangle).The A, B, and C panels show the structure of the catalytic sites (close-up views). (*A*) MalDH type 3 from *Chloroflexus aurantiacus* (Bacteria) (PDB ID. 4CL3), (*B*) Intermediate MalDH (subgroup C) from *Archaeoglobus fulgidus* (Archaea) (PDB ID. 2XOI).

(*C and D*) LDH from *Thermus thermophilus* (Bacteria) (PDB ID. 2V7P, 2V6M being Holo and Apo state, respectively). Residues colored in pink and blue are typical of MalDHs and LDHs, respectively. For the sake of clarity, the helix α1G/α2G is not shown. The nature of the amino acid at position 102 for each enzyme is indicated, but due to the location at a large distance it is not represented. Amino acids are numbered according to the normalized nomenclature of Eventoff (1977). The correspondence between the primary sequence and the normalized numbering for LDH is shown as Supplementary Table S1. Cs means conformational sub state.

The *Thermus thermophilus* LDH enzyme harbors the canonical Q102, D/E199, T246 amino acid signature, the *Chloroflexus aurantiacus* MalDH type 3 contains the typical R102, M199, A/S246 amino acids, while the catalytic site of the *Archaeoglobus fulgidus* MalDH of the intermediate group displays a mix signature: R102, M199, and T246 (fig. 1 and supplementary fig. 1). In allosteric LDHs, H68 and R171 displayed synchronized lateral side chain reorganizations, with H68 mimicking the role of a "door" that controls the localization of R171 within conformational sub states (Cs-in) or outside (Cs-out) the catalytic site (fig. 1*c, d*). In non-allosteric MalDH 3, there is a D at position 68. Sequences from the intermediate groups harbor either D68 or H68 (red triangles, fig. 1 and supplementary fig. 2), suggesting that the D68 to H transition occurred in this group prior to being fixed in LDH.

The structural analysis (fig. 1) showed that the amino acid at position 250 is located in close vicinity to R171 and the amino acid at position 246, in agreement with previous reports indicating it is close to the reactive extremity of NADH (Dalhus et al. 2002; Irimia et al. 2004; Coquelle et al. 2007). Interestingly, the amino acid at position 250 was also proposed to distinguish between LDHs (I250) and MalDH type 3 (P250) (Madern 2002).Yet, the role of the amino acid at this position has never been experimentally analyzed. In light of these considerations, we investigated the evolution of residues at position 68, 102, and 250 along the phylogeny of LDHs, MalDH type 3, and intermediate MalDHs (fig. 1 and supplementary fig. 2).

The mapping disclosed a strong association between R102, P250, and D/Q68 in MalDH type 3, and between Q102,I250, andH68in LDHs (supplementary fig. 1),suggesting these amino acid signatures may be linked to specific enzymatic properties, such as allosteric capacity and substrate recognition. Regarding the intermediate group of MalDH, mixed combinations of LDHs and MalDH type 3 signatures are observed (fig. 1 and supplementary fig. 2). More precisely, most sequences harbor: (i) R102, P250, as MalDH type 3, associated with the H68 observed in LDHs, (ii) I250 and H68, as LDHs, but neither Q102 nor R102, or (iii) I250 as LDHs, D68 as MalDH type 3, but neither Q102 nor R102. While most sequences from the intermediate group display A/S246 like MalDH type 3, some of them harbor H68, R102, and

P250, carries also T246 like LDH sequences (fig. 1 and supplementary fig 2).They provide, therefore, an opportunity to examine the most favorable combination, using a minimal set of evolutionary related mutations, which may turn a non-allosteric MalDH into an allosterized enzyme. The crystal structures of only two MalDH enzymes from the intermediate group that display the H68, R102, T246 and P250 signature sequence are deposited at PDB: 2XOI and 6QSS from the archaea *A. ful* and *Ignicoccus islandicus (I. isl),* respectively (Irimia et al. 2004, Roche et al. 2019). Each display peculiar discrepancies with respect to the canonical tetrameric association that prevails in the LDH/ MalDH super family. The *A. ful* enzyme is a dimer, likely because of a six amino acid deletion at the interface that participates to tetrameric assembly (Madern et al. 2001, Irimia et al. 2004), while the *I. isl* enzyme is a "twisted" tetramer with a major displacement, at the dimer of dimers that make the final assembly (Roche et al. 2019).
To go further, we investigated the role of amino acids at positions 102 and 250 using the enzyme from *A. fulgidus* as template. More precisely, three mutants were designed. The first one, Mutant 1 contains the single R to Q mutation at position 102 (R102Q) that is intended to modify the substrate recognition, from OAA toward PYR making this enzyme an LDH, while the proline in position 250 is unchanged. The second one, Mutant 2, allows to test the effect of the substitution of proline by isoleucine at position 250 (P250I), while the R102 is not modified in order to keep the MalDH functionality unaltered. The third and final one, Mutant 3 (R102Q and P250I), combines both mutations.

Effect of mutations on protein stability and activity profiles.

We first checked that the mutations were without any major effects on the quaternary assembly, fold and stability of the resulting purified enzymes. The Wt *A. ful* MalDH and the three mutants were eluted on a SEC column with a similar profile. As expected for dimeric enzymes, they

displayed a similar elution volume (Ve= 14.5 mL) higher than the value of 13.5 mL corresponding to a tetrameric LDH used as control (supplementary fig. 3).

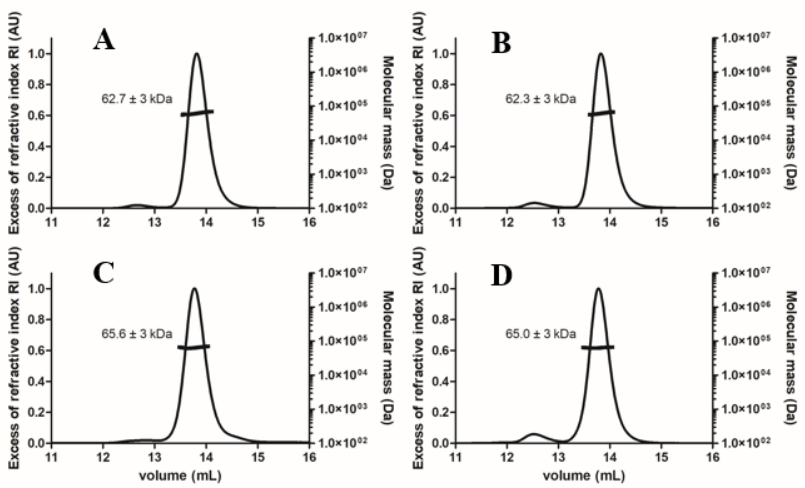

FIG. 2. Oligomeric state determination of the *A. ful MalDH and mutants* using SEC-MALLS analysis. The chromatogram shows the elution profile monitored by excess refractive index (left ordinate axis) and the molecular weight as dashed line (right ordinate axis) derived from MALLS and refractometry measurements. The estimated average molecular weight is indicated on the graph. (*A*) Wt *A. ful* MalDH, (*B*) mutant 1, (*C*) mutant 2, (*D*) mutant 3.

We then monitored their apparent molecular weight using a SEC MALLS analysis and compared them with the theoretical MW of 72 Kda for the dimeric state. All the enzymes displayed similar MW (62-65 kda) demonstrating that they behave as dimeric species in solution (fig. 2).We recorded their CD spectra at 25°C and after an incubation of 15 min at 80°C. The CD spectra displayed strong negative amplitude at 208 and 222 nm and a positive amplitude at 200 nm that reflect a typical folded protein (supplementary fig. 3). After incubation at high temperature, there is no significant variation of amplitude at 222 nm showing that all these enzymes have remained hyperthermophilic. We concluded that mutations on residues at positions 102 and 250 did impact neither the quaternary assembly nor the apparent conformational stability. This is not surprising, because the analysis of the Wt *A. ful* MalDH structure strongly suggests that the two targeted residues are not involved in intra molecular interactions.

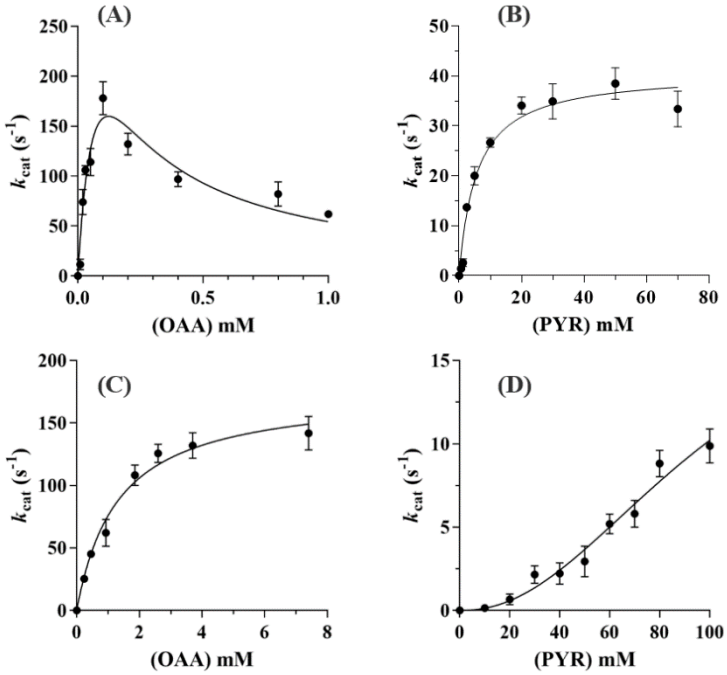

FIG. 3. Catalytic properties of *A. ful* MalDH and mutants at 340K. (*A*) OAA saturation curves for the Wt enzyme carrying R102 and P250, (*B*) PYR saturation curves for the mutant 1 containing Q102 and P250, (*C*) OAA saturation curves for the mutant 2 displaying R102 and I250, (*D*) PYR saturation curves for the mutant 3 having Q102 and I250.

In contrast, the mutations impacted functionality. Wt *A. ful* MalDH displays an enzymatic activity profile that indicates inhibition by an excess of substrate (fig. 3*a*), as it is frequently observed in many MalDHs type 3. The enzyme has a strong affinity for OAA as substrate with K_m values of 100 µM and an enzymatic efficiency in close agreement with previous reports (Langelansvik et al. 1997). We also tested that the Wt *A. ful* MalDH does not use PYR as substrate (Table 1). As anticipated, the single R102Q amino acid replacement in mutant 1 changes substrate recognition from OAA to PYR (fig. 3*b*), a previously reported functional LDH mimicking transformation, which confirms that the amino acid at position 102 should be regarded as the "main specificity residue" between MalDHs and LDHs (Wilk et al. 1988; Cendrin et al. 1993; Boernke et al. 1995; Boucher et al. 2014; Steindel et al. 2016; Katava et al. 2020). However, compared to the Wt enzyme, the mutation decreases by 57-fold the affinity for the new substrate (PYR) and decreases the catalytic efficiency (k_{cat}/K_m) (fig.3 *a*, *b* and Table 1). We also observed that mutant 1 is still able to recognize OAA with a lower efficiency than with PYR (Table 1). This observation suggests that additional mutations are required to swap completely the specificity in MalDH toward a highly efficient LDH (Cendrin et al. 1993; Boernke et al. 1995; Yin and Kirsch 2007). It was out of the scope of this study to investigate this issue in details.

In mutant 2, in which the initial MalDH functionality is conserved, theP250Ireplacement abolishes the inhibition by excess of OAA and the activity profile exhibits a hyperbolic shape (fig. 3*c*).The affinity for OAA was significantly reduced about 31-fold with a K_m value of 1.31 mM suggesting that the P250I replacement has induced a reorganization of the binding site impacting the interaction with the substrate. We did not detect any activity in the presence of PYR with this mutant (Table 1) and the Wt enzyme as it is the case with most of the MalDHs. The k_{cat} value of mutant 2 is lowered compared to the Wt *A. ful* MalDH. Yet, the most striking change of phenotype occurred when the two mutations R102Q and P250I are combined. Indeed, the *A. ful* mutant 3exhibits a sigmoid PYR recognition profile with very high $S_{0.5}$(K_m) values and an important loss of catalytic efficiency (fig. 3*d*, Table 1). Such a phenomenon mimics the typical behavior of many allosteric LDHs which, in the absence of their allosteric effector (FBP), exhibits sigmoid shaped substrate saturation curves, or very low activity at physiological concentration of PYR (Arai et al. 2011). We also tested the capacity of mutant 3 to use OAA and found no activity. Yet, unlike the allosteric LDHs, there is no enzymatic activation with any of the mutants and Wt *A. ful* enzyme in the presence of 0.3 and 3 mM FBP. This was expected because, at variance with the tetrameric organization, the dimeric nature of the investigated proteins does not offer appropriate binding site to FBP. In allosteric LDHs several studies have shown that the allosteric regulation originates in the quaternary structural transition between the T-inactive state and active R- state, in which the tetramers take on extended and compact conformations, respectively (Reviewed in Taguchi 2017). Our data demonstrate that, in the MalDH/ LDH, just a few amino acid mutations mimicking evolutionary events may trigger homotropic activation from a non-allosteric dimeric enzyme.

	K_m or $S_{0.5}$ (mM)	k_{cat} (s^{-1})	k_{cat}/K_m (M^{-1} s^{-1})
Wt (OAA)	0.1	417	4.3×10^6
Wt (PYR)	ND	ND	ND
Mutant 1 (OAA)	14	12	0.9×10^3
Mutant 1 (PYR)	5.6	40	7.1×10^3
Mutant 2 (OAA)	1.3	175	1.3×10^5
Mutant 2 (PYR)	ND	ND	ND
Mutant 3 (OAA)	ND	ND	ND
Mutant 3 (PYR)	100	21	210

Table 1. Kinetics parameters of Wt and mutants *A. fulgidus* MalDH. ND means not detectable

R102 and P250 mutations modify the flexibility of theR171 substrate-binding residue of A. ful MalDH enzymes at functional temperature.

In order to address the relative effect of mutations on the conformational fluctuations of *A. ful* MalDH, we performed a series of Molecular Dynamics (MD) simulations using the Wt and mutant structural models (see methods). We characterized the conformational landscape of Wt *A. ful* MalDH, similar to the R-active state of allosteric LDHs, but as we will show, it can be altered by specific mutations toward transient conformers that mimic the T-*like* inactive state of allosteric LDHs.

In order to characterize the conformational space explored by the R171 side chain, we first recorded various distances between key amino acid positions. This was done at ambient temperature (300 K) and close to the enzyme optimal functional temperature (340K).Recall that, in a given monomer the shorter the distance is between R171 and P141, and most of the R171 side chain is located within the catalytic site, and *vice versa* when the distance between R171 and N181 is considered (Mirror effect) (see fig. 4, close up view). The variation of the distance between R171 and amino acid position 250 on the one hand, and the distance distribution of H68 from the adjacent monomer to the same reference amino acids at positions141, 181 and 250, on the other hand were also monitored. At 300K, the distance distributions are very similar among the various systems (supplementary fig. 4), indicating that the effect of the mutations on the conformational space is not perceptible at ambient temperature.

Raising the temperature to 340K revealed drastic changes (fig. 4). In the Wt enzyme, all the R171 and H68 distance distributions (purple lines) are quite similar indicating that each monomer behaves similarly. The distances are close to those recorded with the crystal structure, showing that (i) R171 side chains are firmly located within the catalytic site, and (ii) H68 is in a “closed” conformation that prevents the R171 side chain to explore the “out” conformational sub-states. With mutant 1(R102Q), the R171 and H68 distance distributions (green lines) are also quite similar in each monomer. Even if the R102Q mutation changes the substrate recognition property as recorded previously, this appear to be without any major consequences on the R171 and H68 local dynamics.

As a result of the P250I mutation, the distance distribution in *A. ful* MalDH mutant 2differ from those observed with the Wt enzyme. In monomer A, the impact is limited (blue lines, fig 4*a*). The R171-P141 distance distribution is broadened and the one with I250 shows two peaks. The R171-N181 distance distribution and H68 distance distribution in monomer B were also not

modified. In contrast, in monomer B, distance distributions for R171 and H68 were strongly modified (blue lines, fig 4*b*). The R171-P141 distance distribution showed two peaks at 17 and 20 A, whereas the "mirror" R171-N181 distribution displayed peaks at 11 and 13 Å, respectively. These measurements indicate that the R171 side chain in mutant 2 no longer protrudes into the catalytic site, as encountered in MalDHs, including the Wt *A. ful* enzyme. The two peaks observed with R171-I250 shows the R171 side chain fluctuates around distinct configurations outside the catalytic site. Note that the H68 distance distributions in the adjacent monomer A is also modified. H68-P141 and H68-N181 change in opposite ways and the H68-P250 distance distribution indicates H68 has moved closer to P250. These measurements show H68 of monomer A has moved in an "open" conformational sub-state, which favors the R171 out sub-state of monomer B.

In mutant 3 that combines both R102Q and P250I mutations (orange lines fig 4), the effect on distance distributions is of wider amplitude. In monomer A, a major structural reorganization of R171 occurred as shown by R171-P141 values, which have increased up to 22 Å, whereas the "mirror"R171-N181 distribution has decreased by 3 Å. The values of 12Å for the R171-I250 distance confirms a major change. As observed previously with mutant 2, the H68 distance distribution in monomer B, indicates the side chain occupied an "open" position. The R171 distance distribution in monomer B indicates no major reorganization.

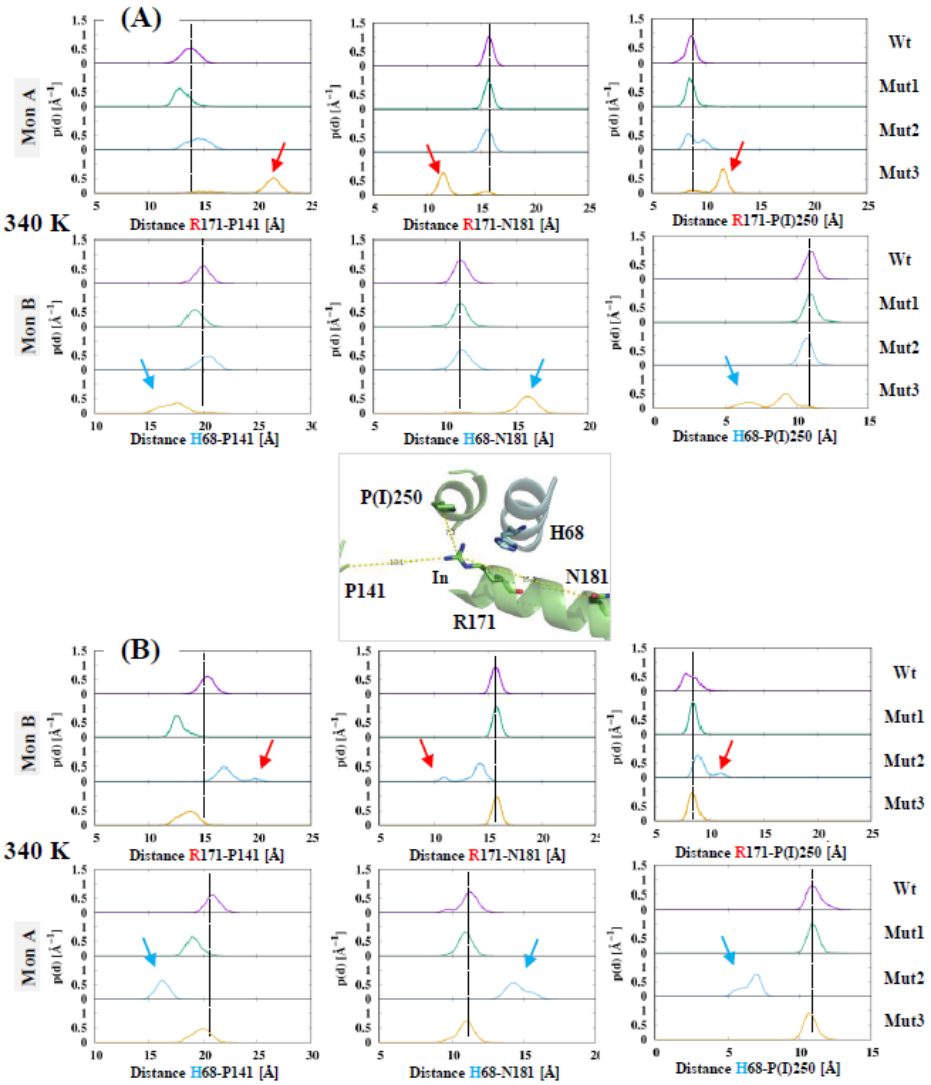

FIG 4. Effect of mutations on the R171 and H68 conformational sub-state sampling at 340K. Probability distributions of the distances between Cγ atoms of R171 and H68 and the Cα atoms of three different residues: P141, left; N181, central; P(I)250, right. The inset shows the position of the considered amino acids in the crystal structure. R171 is inside (in) the catalytic site. (*A*) Fluctuations of R171in monomer A and adjacent H68in monomer B. (*B*) Fluctuations of R171in monomer B and adjacent H68 in monomer A. The dashed line refers to the distance distribution for the Wt *A. ful* MalDH. The color code is purple, green, pale blue, and orange, for Wt *A. ful* MalDH, mutant 1, mutant 2, and mutant 3, respectively. Arrows indicate significant distance deviations with respect to the Wt enzyme.

We concluded that, the P250I mutation induces dynamically important effects on the mobility of substrate binding residue R171.The effect is amplified, in particular at the high functional temperature when in conjunction with the mutation R102Q. In these conditions, R171 protrudes outside the catalytic site and, therefore, mimics the situation encountered in the T-inactive state of allosteric LDHs. This amino acid replacement also has, a major impact on communication between monomers that alternatively can populate R- or T- like catalytic site configurations. The effect of the amino acid replacement P250I propagates to the AB monomer interface and

promotes the sampling of specific conformational states of R171 and H68 side chains. Our results also provide key information about the timescale of conformational fluctuations in the two domains. In fact, we have seen that the distributions (e.g. the distances in mutants 2) are not identical between the two domains; this implies that the reshuffling among main conformations in a single domain exceeds the microsecond timescale that we probe here with our simulations.

Impact of I250 side chain mobility on substrate affinity

With the P250I mutation, a non-polar side chain protrudes in the catalytic site. With mutant 3, which carries the additional R102Q mutation, MD simulation at 340K reveals that the I250 side chain visits three configurations (Cs1, Cs2 and Cs3) (supplementary fig. 5a). As expected, the superposition between the Wt enzyme and the most representative conformers for I250 side chain indicates its location within the catalytic site close to the reactive extremity of NADH (supplementary fig. 5b). The comparison with representative structures of the allosteric *T. the* LDH in the T and R states indicates that Cs3 mimics the T-like state (supplementary fig. 5c, right panel), whereas Cs2 corresponds to the R-like state (supplementary fig. 5d, central panel). Because of a putative steric clash between the NADH reactive extremity (C4 ring carbon) and I250 Cs1, that would hinder the correct geometry requested for an efficient hydride ion transfer, we considered this sub state as unfavorable (supplementary fig. 5d , left panel). We observed that I250 is connected to T246 through van der walls contact with the main chain of amino acid at position 251. Amino acid at position 246 also participate interaction with the substrate (Brochier-Armanet and Madern 2021). T246 conformational sub states in *A. ful* MalDH mutant 3 differ from those observed in the R-active state of an allosteric LDH (supplementary fig. 5). Consequently, in addition to the capacity of R171 to explore a T-like state, none of the favorable conformational subs states combination between I250 and T246 are achieved to ensure strong PYR affinity and high catalytic efficiency in mutant 3.

Mutation of R102 and P250 modify the conformational landscapes of A. ful MalDH at functional temperature.

We now focus our attention on one helix, which displays an important conformational reorganization in allosteric LDHs (Iwata et al. 1994; Coquelle et al., 2007). In the LDH structure representative of the R-active state (PDB accession number 2V7P), the α2F helix is in a rather "flat" position as illustrated in Fig. 5. The substrate-binding residue R171 is in a favorable position to interact with PYR within the catalytic site. In the LDH structure representative of

the T-inactive state (PDB accession number 2V6M), the α2F helix moves "under" with respect to its position in 2V7P and the side chain of R171 is projected outside the catalytic site (Iwata et al. 1994; Coquelle et al., 2007).

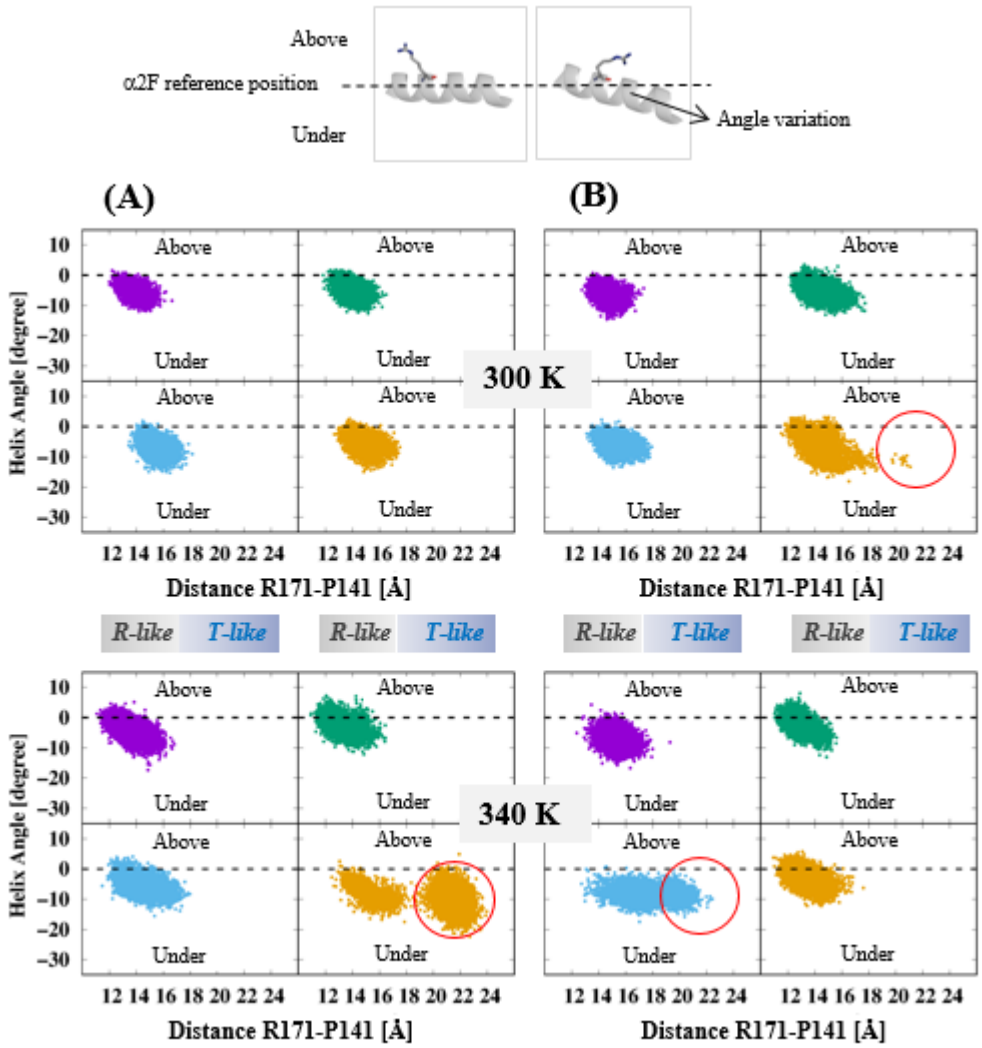

FIG 5. Conformational landscape variation of the α2F helix in *A. ful* MalDH and mutants. The color code is purple, green, pale blue and orange, for Wt *A. ful* MalDH, mutant 1, mutant 2, and mutant 3, respectively. (*A*) Monomer A at 300 K (Top) and 340 K (Bottom). (*B*) Monomer B, same conditions. The top close-up view corresponds to the various α2F helix positions as observed in the *T. the* LDH crystal structures representative of the R-and T- states, left and right images, respectively.

We analyzed whether or not the WT enzyme and mutants were adopting 2V6M-like α2F helical angles during the simulations, and found it was not the case to the exception of mutant 3 (supplementary fig. 6). Then, we drew a two dimensional scatter plot to analyze change of the conformational landscape due to the mutations (Fig 5). It is interesting to note that at 300K, all the enzymes behave in the same way in each monomer. However, in mutant 3, monomer B explores different conformations (red circles). At 340K, the temperature increase allows a more

drastic change in mutant 2 and 3 that carry the P250I mutation. In mutant 2, the scatter plot profile for monomer A is not impacted. In contrast, with monomer B the plot is ellipsoidal showing the number of conformers with both a R171-out and a α2F "under" configuration has strongly increased (red circles). With mutant 3, the monomer A profile shows two separate clouds indicating that conformers with the R171-out and a α2F under configuration are strongly favored (red circles). As with mutant 2, the adjacent monomer profile is not impacted.

We selected two conformers of mutants 2 and 3 along the MD simulations, which displayed strong parameter deviations (red circle in fig. 5) with respect to those of the Wt enzyme, and superimposed their structures with the representative crystal structure of an allosteric LDH in the T-inactive state (fig 6). The apo state LDH from *Thermus thermophilus* (*T. the*) was used (Coquelle et al. 2007).

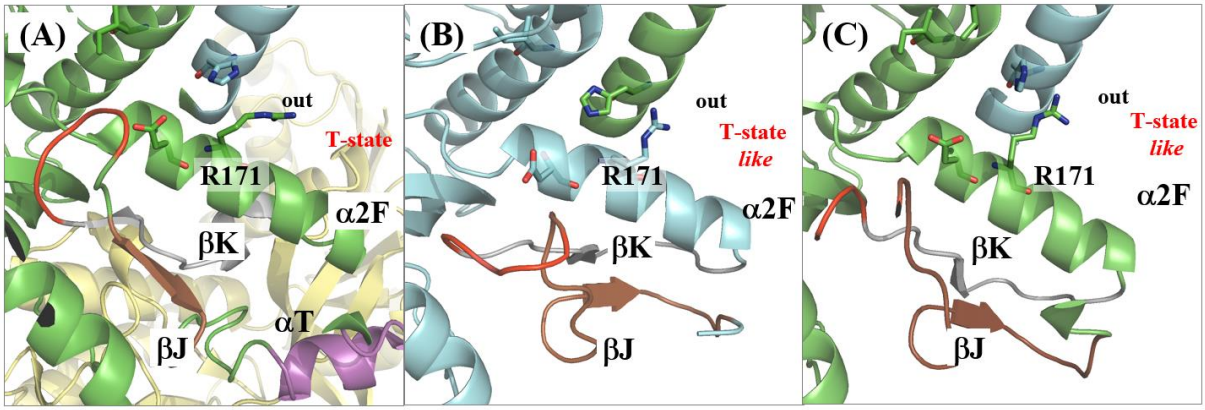

FIG. 6. Structural comparison between mutant 2 and 3 of *A. ful* MalDH, with *T. the* LDH T- state (PDB ID2V6M).(A) Close up view of *T. the* LDH.). Monomer A, B and D are in green, cyan and yellow, respectively. Monomer C is not shown. R171 is outside the catalytic site (out). Several secondary structure elements are identified. (B) Conformers of *A. ful* MalDH mutant 2, from MD simulation at 340K, "189,500ps". (C) Conformers of *A. ful* MalDH mutant 3, from MD simulation at 340K, "750,000 ps".

The structural comparison shows that some conformers of mutants 2 and 3 at 340K display a local reorganization of the α2F helix and R171 that resembles the typical structure of an allosteric LDH in the T- state. These data demonstrate that the P250I mutation is of major importance to change the dynamical properties of *A. ful* MalDH. Not only does it allows R171 to explore a non-competent state for substrate binding, but it also promotes correlated motions between residues at the A-B interface. Note that the capacity of I250 to promote an allosteric like effect as in LDH is strongly amplified when the mutation R102Q, allowing to change functionality, is added.

Effect of mutations on the flexible active site loop.

In numerous crystal structures of LDHs and MalDHs, the active site loop that carries the substrate discriminating amino acid at position 102 has been described in two different conformations (Iwata et al. 1994; Auerbach et al. 1998; Winter et al. 2003; Coquelle et al. 2007; Arai et al. 2010, González et al. 2018). These correspond to either open or closed conformations, as observed in the Apo or Holo structures, respectively. The open position is shown in Fig 7A. It corresponds to the crystal structure of Wt *A. ful* MalDH. In this case, the R102 and R109 side chains are far away from the catalytic crevasse.

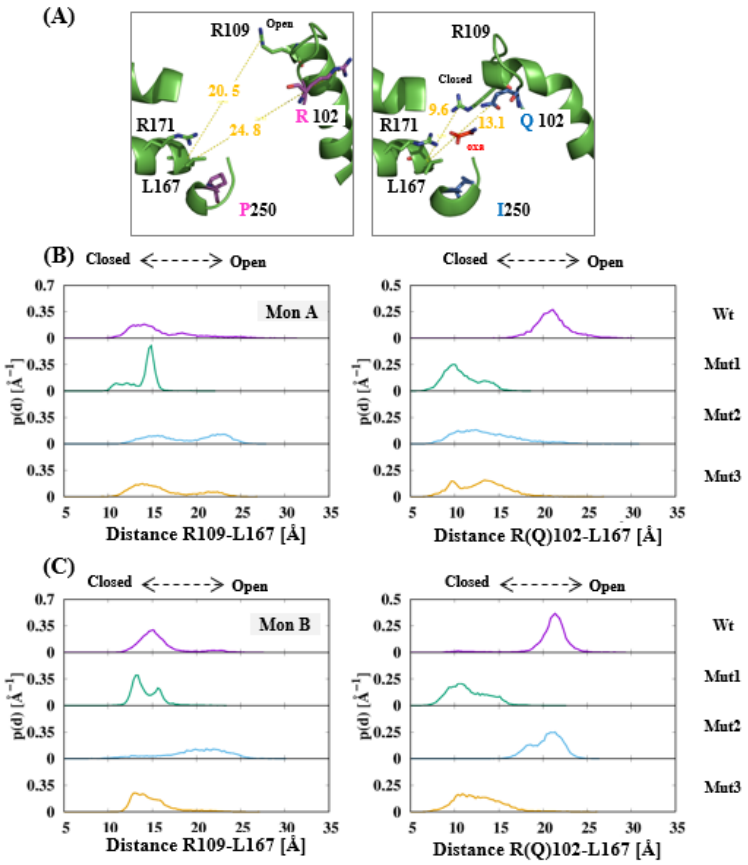

FIG. 7. Mobile loop fluctuations in Wt *A. ful* MalDH and mutants at 340K. The figure shows the probability distributions of the distances between CG atoms of R(Q)102 and R109 and the Cα atoms of L167. (*A*) The left and right small insets show the position of the various amino acids considered in *A. ful* MalDH and *T. the* LDH crystal structures, respectively. (*B*) Fluctuations in monomer A. (*C*) Fluctuations in monomer B. The color code is purple, green, pale blue and orange, for Wt *A. ful* MalDH, mutant 1, mutant 2 and mutant 3, respectively.

Their distances with respect to the α2F helix extremity, monitored using the conserved position L167, are larger than 20 Å. The typical closed position for the loop is observable in the crystal structure of *T. the* LDH in the Holo state (fig. 7*a*). In this case, the side chains of R109 and

Q102 are located closer to the α2F extremity, with values 9.6 and 13.1 Å, respectively. Note that in numerous structures the loop is not modeled because of a too high flexibility.

We monitored these distances in the simulations of the Wt *A. ful* MalDH and mutant systems (fig. 7*a, b*). At 340 K, for each monomer, in the Wt enzyme, the distance L167-R102 shows that the R102 side chain remains far away from the catalytic site, whereas the L167-R109 distance (around 15 Å) indicates a situation slightly different from the crystallographic structure suggesting a local distortion that favors the approach of R109 toward the catalytic site. In mutant 1, for both monomers, the distance distribution for L167-R109 is globally unchanged with a distribution in a range 13-15 Å. In contrast, the L167-Q102 distribution is shifted toward lowest values than in the Wt enzyme, a situation that mimics the situation observed in LDH crystal structure when the substrate analog is bound (Holo state). In mutant 2, the L167-R109 distribution shows two peaks in monomer A, indicating that the side chain fluctuates between open and closed conformations. In Monomer B, the R109 is in a rather open position. In monomer A, the L167-R102 distance distribution agrees with a closed conformation for R102. In contrast, the side chain of R102 occupies the open position in monomer B. In mutant 3, the distance distribution that accounts for R109 and Q102 positions suggests that their side chains are in a closed-like conformation.

Our data suggest that in the Wt and mutants of *A. ful* MalDH, fluctuations of the mobile loop in the Apo state are strongly constrained by electrostatic interactions between R(Q)102, R109 and R171. When R102 is present, a dominant repulsive regime between three positive charges maintains the loop in an open-like state. With Q102, the charge repulsion effect is low and the loop can more easily explore the closed-like state. The data also show that the loop movements are better described by a twist rather than by a rigid translation.

Discussion.

Strongly inspired by the pioneering concept linking the capacity of proteins to evolve and conformational dynamics proposed by Tokuriki and Tawfik (2009), we addressed the question concerning the origin of allostery in LDH.

Allosteric regulation in LDHs fits the MWC model (Monod et al. 1965), in which an allosteric enzyme fluctuates (even in absence of effector) between at least two conformational states –R (relaxed, with low affinity for the substrate) or T (tense, with high substrate affinity). (Taguchi 2017 and reference therein). Apo and Holo crystal structures of LDHs representative of the T and R states, show that the position of the side chain of the strictly conserved R171, a relevant

proxy for the T or R states (Iorio et al 2021), is always found either outside or inside the catalytic site of all monomers.

First, by combining a phylogenetic and structural analysis we suggested that amino acid replacements of two amino acid position (68 and 250) located within the catalytic pocket would have had a strong influence on the transition between non-allosteric MalDHs type3 and canonical allosteric LDHs. Our phylogenetic analysis, based on Brochier-Armanet and Madern (2021), showed the predominant occurrence of H68 and D68 in the intermediate group of MalDHs, suggesting different abilities regarding allostery (fig. 8), with a pre-existing capacity in enzymes harboring H68 prior to the fixation of this amino acid in LDHs. LDH crystal structures showed that the conformational fluctuations of R171 rely on the presence H68 that sustains the flexibility at the monomer A -monomer B interface, and allows the R171 side chain to swing out of the catalytic site. In canonical LDH, the replacement of H68 by D68 contributes to a salt-bridge formation with R171, which abolishes the sigmoid activity profile of the allosteric bacterial LDH mutant from *Lactobacillus casei* (Arai et al. 2011). The crystal structure of non-allosteric LDHs from *Lactobacillus pentosus* (PDB code: 1EZ4) indicates a D at position 68 that also maintain R171 in the R-active position (Uchikoba et al. 2002). In non-allosteric MalDH type 3, representative crystal structures (PDB code: 4CL3, 4BGV) show that when a negatively charged residue (E68) establishes a salt-bridge with R171, its side chain protrudes within the catalytic site. MDS simulation using 4CL3, did not reveal any changes from the R-active toward the T-inactive state at high functional temperature (Kalimeri et al. 2014). These observations demonstrate that the presence of a histidine at position 68 strongly contributes to establish the allosteric phenotype.

Second, we analyzed the consequence of the P250I substitution in an enzyme from the intermediate group that carries H68, with *A. ful* MalDH as model. Here, the P250I mutation has allowed the I250 side chain to sample several conformations within the catalytic site, which mimic those existing in the T- and R-states of an allosteric LDH. Several studies have shown that the proline could be seen as a small switch that modulates the allosteric behavior (Collins et al. 1995; Rodicio et al. 2000; Weyand et al. 2002; Vogel et al. 2006; Wei et al. 2014). Because the proline ring restricts the protein backbone flexibility, its replacement by another amino acid is not neutral. This mutation should be considered as a dynamics-enhancing replacement that rendered enzymes from the intermediate group prone to evolve toward allostery prior to its fixation in canonical LDH.

Third, we observed that while the *A. ful* MalDH mutant 2 differs from the Wt enzyme only by one amino acid (P250I), it exhibited a lower affinity for OAA. A strong decrease in affinity for

PYR was also detected in *A. ful* MalDH mutant 3. We analyzed by MDS that introducing I250 side chain in the catalytic site has an unexpected unfavorable consequences of the T246 conformers sampling, a residue also involved in substrate discrimination that should favors PYR recognition (Brochier-Armanet and Madern 2021, reference therein). It confirms the hypothesis done by Brochier and Madern (2021), which stipulates that the appearance of I250 together with the A/S to T replacement at position 246 in enzymes of the intermediate group, contributed in the extinction of OAA recognition during the MalDH to LDH functional transition. We suggest that the *A. ful* mutant 3 (P250I and R102Q) low catalytic efficiency and low substrate affinity are caused by an increased number of unproductive conformers of the active site related to I250 fluctuations. Very recently, it has been shown that unfavorable conformations of amino acid side chains can drive major structural reorganization in a JNK interacting protein (Mariño Pérez et al. 2022).

Fourth, we notice that these two substitutions occurred prior to the critical replacement of R at position 102 by Q in the stem of canonical LDH clade, considered as the main discriminating residue for functionality between MalDH and LDH (Wilk et al. 1988; Cendrin et al. 1993; Boernke et al. 1995; Boucher et al. 2014; Steindel et al. 2016; Katava et al. 2020; Brochier-Armanet and Madern 2021). Therefore, we assume that owing to its pleiotropic effect, the amino acid replacement P250I was one of the strongest drivers of phenotypic evolution within the MalDH / LDH superfamily. Notice that the "allosterized" capacity of the *A. ful* induced by P250I was enzymatically detectable only in presence of the extra R102Q mutation that acts at the level of substrate recognition. In addition, by using MDS, we revealed that electrostatic property changes, induced by the R102Q mutation, promoted a structural distortion of the mobile binding site loop that modulates the open/closed propensity in the Apo state. We propose that this mutation not only serves functional evolution, but in combination with I250, enlarges the conformational landscape of the protein. The observation is in agreement with a work showing that allosteric propensity is coupled with loop dynamics (Galdadas et al. 2021).Yet, the combination on a MalDH scaffold of H68, Q102, T246 and I250 was not sufficient to design a homotropicaly activated LDH with high catalytic efficiency. This is likely due to the phenomenon of epistasis, i.e. the context-dependence of mutation in the relationship between sequence changes and phenotypic variation (Poelwijk et al. 2016), meaning that additional changes are required to fully achieve the MalDH / LDH functional transition. Here, the shorter sequence of *A. ful* MalDH, compared to most of its homologues, has reorganized the structure (see below) so that the complete putative effect of allosteric LDH-like mutations was not fully transferable. Studies have shown that the accumulation of amino acid substitutions

allow the recruitment and optimization of a preexisting low-level property in a protein scaffold, creating proteins with high latent evolutionary potential (i.e. marked ability to evolve new properties) (see (Khersonsky and Tawfik 2010) and references therein).The potentiality to evolve of these enzymes with latent properties can be controlled either by a relaxed or a stringent negative trade-off between the initial and final function (Khersonsky and Tawfik 2010). This then allows the promiscuous intermediate to change their properties with very few amino acid substitutions (Thornton et al. 2003; Wouters et al. 2003; Zou et al. 2015; Otten et al. 2018). The various steps that relate the MalDH/LDH evolution fit well these fundamental principles.

Fifth, our data based on the MalDH / LDH superfamily add precious information for understanding the evolution of allostery. By exploiting the resolution of MDS, we found that, by introducing two LDH like mutations into a dimeric archaeal MalDH from the intermediate group, the resulting protein homotropicaly activated by PYR starts visiting, even in the absence of any ligands, new configurational states relevant for allosteric regulation (see the grey inset in fig. 8). This few mutations could be considered as permissive for the selection of a new phenotype as previously observed with other allosteric enzymes (Kuo et al. 1989; Stebbins et al. 1992; Farsi et al. 2012). Some studies suggested that allosteric property of modern proteins arose in ancestral proteins with a latent capacity for allosteric modulation (Reynolds et al. 2013; Coyle et al. 2013; Hadzipasic et al. 2020), while others proposed that allosteric regulation emerged from non-allosteric extinct ancestral enzymes (Mas-Droux et al. 2006; Raman et al. 2016; Schupfner et al. 2020). Two studies based on ancestral sequence reconstruction have analyzed the selection of allostery in contemporary pyruvate kinases and steroid receptors. This is due to mutations at some key positions that exist within interaction networks and which, may rewire the network, subsequently altering transmission of the signal (Johnsen et al. 2019; Okafor et al. 2020). Different studies provided convincing explanations to explain why few mutations are responsible for changes in allosteric capacity. This is because in enzymes, the dynamical process is hierarchical and covers different times scale that influence functionality and allostery (Frauenfelder et al. 2001; Wrab et al. 2011; Choy et al. 2017; Wolf et al. 2021; Fleishman and Horovitz 2021; Makurat et al 2022; Madhu et al. 2022). Because of this hierarchy, very short time scale dynamics, due to simple side chain fluctuations of a single residue can influence reorganization between the T-and R states (Zhou et al. 2003, Fujiwara et al. 2017, Iyer et al. 2021). How the enzymatic activation (heterotropic activation) of LDHs by the allosteric effector (FBP) evolved (concomitantly or successively) requires additional investigations.

Finally, we discuss the allosteric capacity in MalDH and LDH superfamily in the light of current concepts of allostery. The initial descriptive phenomenological models of allostery are the MWC and KNF models (Monod et al. 1965; Koshland et al. 1966). In the former, all monomers of the oligomeric enzyme are in the same state, being either T- or R-; whereas in the latter that may exist as a mixture of both states. Several structural studies based on the Wt states of allosteric LDHs have suggested that they obey the MWC model in which all monomers are in the same state (Iwata et al. 1994; Auerbach et al. 1998; Winter et al. 2003; Coquelle et al. 2007; Arai et al. 2010). However, by introducing mutations in the hinge regions of allosteric *T. the* LDH, it has been possible to observe a strong structural heterogeneity between monomers in crystal structures caused by a change in enzyme flexibility (Colletier et al. 2012).The "allosterized" *A. fulgidus* mutant 2 behavior agrees with the phenomenological KNF descriptive model of allostery, in which ligand binding induces sequential conformational changes within the oligomeric enzyme that may exist as a mixture of T and R states (Fersht 1999). The differences we observed are not antagonistic. Indeed, in the recent and integrative ensemble model of allostery, the allosteric character of an enzyme is determined by the redistribution of the occupancy probabilities of different conformational states (Wrabl et al. 2011, Motlagh et al. 2014). We propose that the different apparent behaviors are due to different oligomeric states of LDH, which are always tetrameric, while the "allosterized" *A. ful* mutants are dimeric. Indeed, in the dimeric *A. ful* MalDH, there is a 6 amino acids deletion that prevents the formation of an equivalent secondary structural element (see αT, in fig. 6) as in tetrameric MalDHs or LDHs. In allosteric LDHs, this helix contributes to i) the allosteric core and ii) the FBP-binding site formation, and also helps to establish the interface, between the dimer of dimers that glues the tetrameric scaffold (Auerbach et al. 1988; Coquelle et al. 2007; Iorio et al. 2021). In allosteric LDHs, mutations that target this helix have strong influence on the R-T equilibrium (Colletier et al. 2012). We propose that the presence or absence of this structural element drastically controls the propagation of the changes induced by mutations favoring allosteric regulation in LDHs. In a recent study, Brochier-Armanet and Madern (2021) proposed that the dimeric state of enzyme from the intermediate group is the minimal functional unit in which the homotropic activation has evolved, our present study demonstrated it the case. Heterotropic activation, on the other hand, requires the tetrameric scaffold.

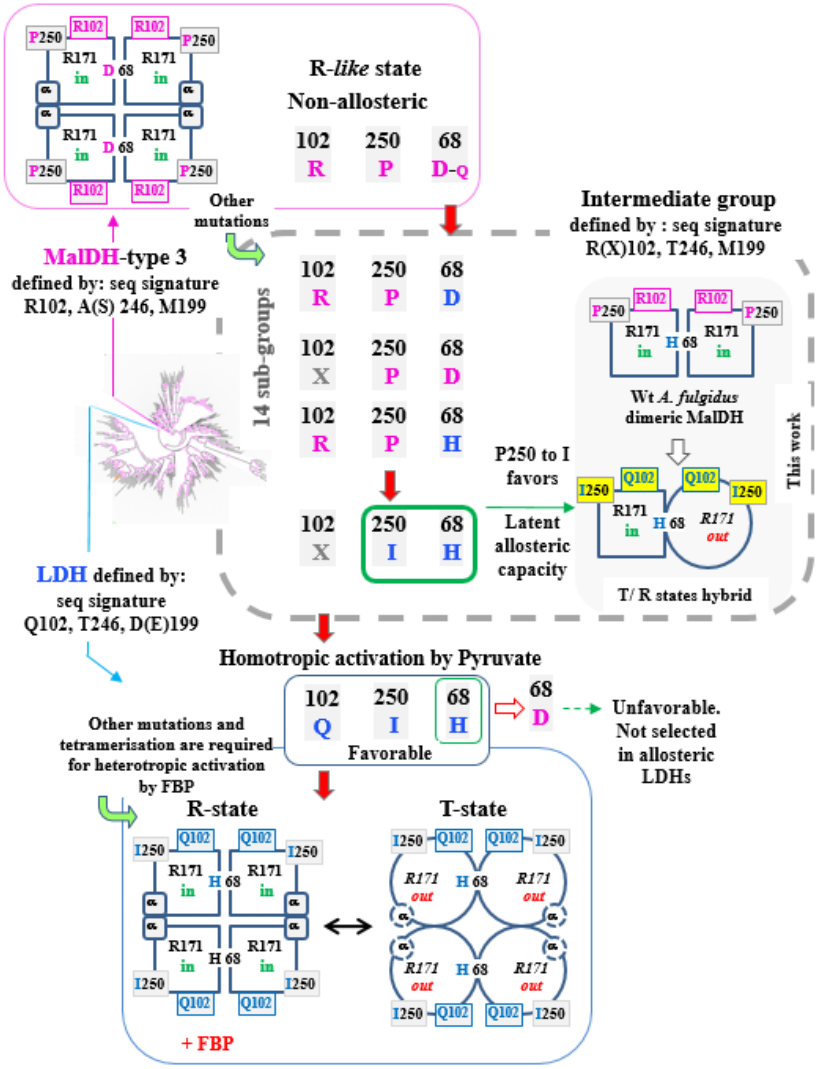

FIG. 8. Scheme of functional and dynamical evolution associated with the emergence of canonical LDHs from MalDH type 3.The three mains groups of enzymes (MalDH type 3, canonical LDH, and intermediate enzymes) are defined according to phylogenetic analyses (Brochier-Armanet and Madern 2021). The evolution of amino acid at key positions (i.e. 68, 102, and 250) is indicated. The active (R-) an inactive (T-) state for a monomer in a given enzyme is represented by a square and a circle, respectively. An amino acid colored in pink or in blue indicates a MalDH or an LDH characteristic, respectively. *In* and *out*, refers to the R171 side chain position within or outside the catalytic site, respectively. The red arrow shows the trajectory of key amino acid replacements requested to facilitate the evolution of non-allosteric MalDH toward LDH, in which allosteric regulation can emerge. The inset in grey summarized the effect of the P250I mutation probed in this work. The consequence of H68D mutation in an allosteric LDH is indicated.

Materials and Methods.

Phylogenetic analyses

The multiple alignment and the maximum likelihood phylogeny of the LDH / MalDH type 3 part of the LDH/MalDH superfamily have been obtained from Brochier-Armanet and Madern (2021). The mapping amino acids residues at position 68, 102, 246, and 250 was on the tree was performed using iToL v.6.4 (Letunic and Bork, 2021).

Cloning of *A. fulgidus* MalDH.

A gene encoding the malate dehydrogenase of *A. fulgidus (*NCBI Reference Sequence: WP_010878358.1) with codons optimized for expression in *Escherichia coli* was synthesized and subcloned into pET-20a by Gencust. The various mutants used in this study were also constructed by the supplier. The NdeI and BamHI cloning sites were used for cloning.

Protein expression and purification.

E. coli BL21 DE3pLyS competent cells transformed with pET-20 expression vector encoding *A. ful* MalDH gene, and mutants were selected by growth on LB agar plates containing 100 µg mL^{-1}ampicillin. A single colony was grown overnight at 37°C in 50 mL^{-1} LB medium at the same concentration of antibiotic. 20 mL of these cultures were then used for inoculation of a 2 liter LB medium containing 100 µg mL^{-1} ampicillin. The cells were cultivated at 37°C until an OD_{600} of 0.6 was reached. Isopropyl B-D-1-thiogalactopyranoside (IPTG) was added at a final concentration of 0.5mM to induce expression and the culture was incubated for 4 hours at 37°C. Bacterial cells were harvested by centrifugation at 6000 g for 20 minutes at 4°C. The pellet was suspended in 40 mL of 50 mM Tris-HCl pH 7.4 containing 50 mM NaCl (Buffer A). Prior cell disruption, 5 µg mL^{-1} of DNAse and $MgCl_2$ to final concentration of 10mMwas added to the cell suspension. The preparation was cooled at 4°C and lysed by sonication (Branson sonicator). Six cycles of continuous sonication at 50 % amplitude were applied during 30 s. Between each pulse, the solution was kept on ice for one minute. The extract was then centrifuged at 13000 g for 30 min at 4°C. The supernatant was further incubated at 70°C for 30 min and the thermally unfolded proteins were removed by centrifugation. The extract was loaded on a Q sepharose column (2x10 cm) equilibrated with Buffer A. *A. ful* MalDH and mutants were eluted with a linear gradient from 0 to 0.8 M NaCl in Buffer A. The active fractions containing the enzyme were pooled, concentrated and loaded on a Superpose 12 gel-filtration column (GE Healthcare) and eluted with Buffer A. The purity of enzymes was

checked by SDS gel electrophoresis. The enzymes were concentrated at 20 mg mL^{-1}in Buffer A and stored at 4°C.

Enzymatic assay and protein determination

The reduction of oxaloacetate to malate of *A. ful* MalDH and mutants was measured in 500 µL of 50 mM K_2HPO_4/KH_2PO_4 pH 7.0 and supplemented with 50 mM NaCl. The reduction of pyruvate to lactate was determined in 500 µL of 2-(N-morpholino) ethane sulfonic acid (MES) pH 6.0 supplemented with 50 mM NaCl. The reaction was monitored spectrophotometrically at 340 nm by following the oxidation of NADH (0.5 mM) on a Jasco 540 at 70°C. To record the enzymatic profile of both enzymes, various substrate concentrations were tested. The data were analyzed using Michaelis-Menten or allosteric sigmoidal equations in GraphPad Prism version 7.03. The protein concentration was estimated from the absorbance at 280 nm using a Nanodrop 2000(Thermo Scientific), with molecular weight and extinction coefficient calculated using the server https://web.expasy.org/protparam.

Circular dichroism

Far-UV CD measurements were carried out on a JASCO J-810 thermostated spectropolarimeter. Far-UV spectra were recorded in 0.10-cm path length quartz cells. The spectra shown in this work represent the average of three accumulated consecutive scans. The protein concentration was 0.3 mg/ ml.

Determination of native molecular masses of the purified enzymes.

Size Exclusion Chromatography was carried out with a flow rate of 0.5 $mL.min^{-1}$ on an ENrich™ SEC650 10x300 gel-filtration column (Biorad). Calibration of the column was performed with the gel filtration standard from Biorad. Direct comparison of the elution profiles was achieved using the Compare mode of the BioLogic FPLC operating system (Biorad).

Size Exclusion Chromatography - Multi Angle Laser Light scattering (SEC-MALLS).

SEC combined with online detection by MALLS and refractometry (RI) was used to measure the absolute molecular mass of proteins in solution. The SEC run was performed using an Enrich 650 column (Biorad) equilibrated with a buffer composed of 50 mM Tris-HCl pH7.2 and 50 mM NaCl. Separation was performed at room temperature and 50 µl of protein sample, concentrated at ~1mg ml^{-1}, was injected with a constant flow rate of 0.5 ml^{-1} min^{-1}. Online MALLS detection was performed with a DAWN-HELEOS II detector (Wyatt Technology

Corp.) using a laser emitting at 690 nm. Protein concentration was determined by measuring the differential refractive index online using an Optilab T-rEX detector (Wyatt Technology Corp.) with a refractive index increment *dn/dc* of 0.185 ml^{-1} g^{-1}. Weight-averaged molecular weight (Mw) determination was done with the ASTRA6 software (Wyatt Technologies) and curve was represented with GraphPad Prism.

Molecular Dynamics

We used the approach that we developed in a previous study aimed to analyse the thermal dependent allosteric behaviour of two LDHs (Iorio et al. 2021). All-atom Molecular Dynamics simulations of the Wt *A. fulgidus* MalDH and three mutants were performed. The simulations were started from the crystallographic structure (2X0I) and homology-based models. Structural models of *A. ful* mutants were generated using the Swiss model server (https://swiss model.expasy.org/) (Waterhouse et al. 2018). Careful inspection of the crystallographic structure and the homology models did not reveal significant differences.All the simulations were done using the APO states and were carried out in the NPT ensemble at ambient pressure, 1 atm, using the GROMACS 2018 software (Vander Spoel et al. 2005; Abraham et al. 2015), the Charmm36 force field for proteins (Huang et al. 2017) and the TIP3P three points water model. Ions were added to the simulation boxes to neutralize the systems. After the equilibration phase, the systems were allowed to evolve at two temperatures, 300 K and 340 K, for 1 μs with a time step of 2 fs.

Two dimensional scatter plots were obtained in the following way.We first aligned α2F of the Wt enzyme (PDB accession number 2XOI) with the X axis of the simulation box, this allows to create a reference state. The orientation of the helix was given by the vector joining Cα atoms of residues 167 and 181 (Normalized numbering), taken as the *extrema* of the helix. Then, by using the Cα atoms of all residues in a monomer, we aligned each monomer in the MD trajectory with the crystallographic structure of the reference state using a fitting procedure. The angle between the helix in the MD trajectories and the reference state (from the X-axis aligned reference structure), is defined as that formed by the projection of the helix vector in the MD simulations on the X -Z plane with the reference vector of the crystallographic structure. The computed values of the helix angle and the R171-P141 distance were combined to draw a scatter plot that is useful to recognize the conformational changes representative of the R- or T-like states.

Author contributions

DM and FS conceived the project. DM performed samples preparation, SEC analysis, enzymatic measurements and CD spectroscopy; CM performed SEC MALLS experiments. CBA and DM conducted evolutionary analyses. AI and FS performed the molecular simulation. All the authors analyzed the data and wrote the manuscript.

Acknowledgements

The authors acknowledge funding by Agence Nationale de la Recherche (ANR) (program AlloAnc, ANR-16-CE11-0011; AlloSpaceANR-21-CE44-0034-01).IBS acknowledges integration into the Interdisciplinary Research Institute of Grenoble (IRIG, CEA). FS acknowledges the financial support by the Initiative d'Excellence program from the French State (Grant DYNAMO, ANR-11-LABX-0011-01, and CACSICE, ANR-11-EQPX-0008). The work was performed using HPC resources from GENCI [CINES, TGCC, IDRIS] (grant X20206818) and from LBT.

We also acknowledge Pr Paul Schanda and Dr Giuseppe Zaccai for helpful discussions and reading of the manuscript.

Conflict of interest

The authors declare that they have no conflicts of interest with the contents of this article.

The data are available in the article and its online supplementary material. The MDS trajectories are accessible using the DOI 10.5281/zenodo.6380887.

https://zenodo.org/record/6380887#.YjxRATXjKUk

References.

Abraham MJ, Murtola T, Schulz R, Páll S, Smith JC, Hess B, Lindahl E. 2015. Gromacs: High performance molecular simulations through multi-level parallelism from laptops to supercomputers. *Software X*. 1:19-25.

Adeva-Andany M, López-Ojén M, Funcasta-Calderón R, Ameneiros-Rodríguez E, Donapetry-García C, Vila-Altesor M, Rodríguez-Seijas J. 2014. Comprehensive review on lactate metabolism in human health. *Mitochondrion*. 17:76-100.

Arai K, Hishida A, Ishiyama M, Kamata T, Uchikoba H, Fushinobu S, Matsuzawa H, Taguchi H. 2002. An absolute requirement of fructose 1, 6-bisphosphate for the *Lactobacillus casei* L-lactate dehydrogenase activity induced by a single amino acid substitution. *Protein Eng.* 15(1):35-41.

Arai K, Ichikawa J, Nonaka S, Miyanaga A, Uchikoba H, Fushinobu S, Taguchi H. 2011. 1 molecular design that stabilizes active state in bacterial allosteric L-lactate dehydrogenases. *J Biochem*. 150(5):579-591.

Arai K, Ishimitsu T, Fushinobu S, Uchikoba H, Matsuzawa H, Taguchi H. 2010. Active and inactive state structures of unliganded Lactobacillus casei allosteric L-lactate dehydrogenase. *Proteins*. 78(3):681-694.

Auerbach G, Ostendorp R, Prade L, Korndörfer I, Dams T, Huber R, Jaenicke R. 1998. Lactate dehydrogenase from the hyperthermophilic bacterium *Thermotogamaritima*: the crystal structure at 2.1 Å resolution reveals strategies for intrinsic protein stabilization. *Structure*. 6(6):769-781.

Biddle JW, Martinez-Corral R, Wong F, Gunawardena J. 2021. Allosteric conformational ensembles have unlimited capacity for integrating information. *Elife*. 10:e65498.

Boernke WE, Millard CS, Stevens PW, Kakar SN, Stevens FJ, Donnelly MI. 1995. Stringency of substrate specificity of Escherichia coli malate dehydrogenase. *Arch BiochemBiophys*. 322(1):43-52.

Boucher JI, Jacobowitz JR, Beckett BC, Classen S, Theobald DL. 2014. An atomic-resolution view of neofunctionalization in the evolution of apicomplexan lactate dehydrogenases. *Elife*. 3:e02304.

Brochier-Armanet C, Madern D. 2021. Phylogenetics and biochemistry elucidate the evolutionary link between l-malate and l-lactate dehydrogenases and disclose an intermediate group of sequences with mix functional properties. *Biochimie*. 191:140-153.

Bur D, Clarke T, Friesen JD, Gold M, Hart KW, Holbrook JJ, Jones JB, Luyten MA, Wilks HM. 1989. On the effect on specificity of Thr246-Gly mutation in L-lactate dehydrogenase of *Bacillus stearothermophilus*. *Biochem Biophys Res Commun.* 161(1):59-63.
Burgner JW 2nd, Ray WJ Jr. 1984. On the origin of lactate dehydrogenase induced rate effect. *Biochemistry*. 23: 3636-3648.
Chapman AD, Cortés A, Dafforn TR, Clarke AR, Brady RL.1999. Structural basis of substrate specificity in malate dehydrogenases: crystal structure of a ternary complex of porcine cytoplasmic malate dehydrogenase, alpha-ketomalonate and tetrahydoNAD. *J Mol Biol*. 285(2):703-712.
Choy MS, Li Y, Machado LESF, Kunze MBA, Connors CR, Wei X, Lindorff-Larsen K, Page R, Peti W. 2017. Conformational Rigidity and Protein Dynamics at Distinct Timescales Regulate PTP1B Activity and Allostery. *Mol Cell*. 65(4):644-658.e5.
Clarke AR, Wigley DB, Chia WN, Barstow D, Atkinson T, Holbrook JJ. 1986. Site-directed mutagenesis reveals role of mobile arginine residue in lactate dehydrogenase catalysis. *Nature*. 324:699-702.
Clarke AR, Wilks HM, Barstow DA, Atkinson T, Chia WN, Holbrook JJ. 1988. An investigation of the contribution made by the carboxylate group of an active site histidine-aspartate couple to binding and catalysis in lactate dehydrogenase. *Biochemistry*. 27: 1617-1622.
Colletier JP, Aleksandrov A, Coquelle N, Mraihi S, Mendoza-Barberá E, Field M, Madern D. 2012. Sampling the conformational energy landscape of a hyperthermophilic protein by engineering key substitutions. *Mol Biol Evol*. 29(6):1683-1694.
Collins RA, McNally T, Fothergill-Gilmore LA, Muirhead H. 1995. A subunit interface mutant of yeast pyruvate kinase requires the allosteric activator fructose 1,6-bisphosphate for activity. *Biochem J*. 310 (Pt 1):117-123.
Coquelle N, Fioravanti E, Weik M, Vellieux F, Madern D. 2007. Activity, stability and structural studies of lactate dehydrogenases adapted to extreme thermal environments. *J Mol Biol*. 374(2):547-562.
Coyle SM, Flores J, Lim WA. 2013. Exploitation of latent allostery enables the evolution of new modes of MAP kinase regulation. *Cell*. 154(4):875-887.
Dalhus B, Saarinen M, Sauer UH, Eklund P, Johansson K, Karlsson A, Ramaswamy S, Bjørk A, Synstad B, Naterstad K, Sirevåg R, Eklund H. 2002. Structural basis for thermophilic protein stability: structures of thermophilic and mesophilic malate dehydrogenases. *J Mol Biol*. 318(3):707-721.

Deng H, Vu DV, Clinch K, Desamero R, Dyer RB, Callender R. 2011. Conformational heterogeneity within the Michaelis complex of lactate dehydrogenase. *J Phys Chem B.* 115(23):7670-7678.

Deng H, Zheng J, Clarke A, Holbrook JJ, Callender R, Burgner JW 2nd. 1994. Source of catalysis in the lactate dehydrogenase system. Ground-state interactions in the enzyme-substrate complex. *Biochemistry*. 33(8):2297-2305.

Eventoff W, Rossmann MG, Taylor SS, Torff HJ, Meyer H, Keil W, Kiltz HH.1977. Structural adaptations of lactate dehydrogenase isozymes. *Proc Natl Acad Sci U S A.* 74(7):2677-81.

Farsi Z, Pein H, Pazhang M, Zareian S, Ranaei-Siadat SO, Khajeh K. 2012. Conferral of allostery to Thermus sp. GH5 methylglyoxal synthase by a single mutation. *J Biochem*. 152(6):531-538.

Feldman-Salit A, Hering S, Messiha HL, Veith N, Cojocaru V, Sieg A, Westerhoff HV, Kreikemeyer B, Wade RC, Fiedler T. 2013. Regulation of the activity of lactate dehydrogenases from four lactic acid bacteria. *J Biol Chem.* 288(29):21295-21306.

Fersht A. 1999. Structure and mechanism in protein science. New York: W.H. Freeman

Fersht, A. 1985. Enzyme structure and mechanism. New York: 2nd edition Freeman and Co.

Fleishman SJ, Horovitz A.2021. Extending the New Generation of Structure Predictors to Account for Dynamics and Allostery. *J Mol Biol*. 433(20):167007.

Frauenfelder H, McMahon BH, Austin RH, Chu K, Groves JT. 2001. The role of structure, energy landscape, dynamics, and allostery in the enzymatic function of myoglobin. *Proc Natl Acad Sci U S A*. 98(5):2370-2374.

Fujiwara S, Chatake T, Matsuo T, Kono F, Tominaga T, Shibata K, Sato-Tomita A, Shibayama N. 2017. Ligation-Dependent Picosecond Dynamics in Human Hemoglobin As Revealed by Quasi elastic Neutron Scattering. *J Phys Chem B.* 121(34):8069-8077.

Galdadas I, Qu S, Oliveira ASF, Olehnovics E, Mack AR, Mojica MF, Agarwal PK, Tooke CL, Gervasio FL, Spencer J, Bonomo RA, Mulholland AJ, Haider S. 2021. Allosteric communication in class A β-lactamases occurs via cooperative coupling of loop dynamics. *Elife*.10:e66567.

Garvie EI. 1980. Bacterial lactate dehydrogenases. *Microbiol Rev*. 44(1):106-139.

González JM, Marti-Arbona R, Chen JCH, Broom-Peltz B, Unkefer CJ. 2018. Conformational changes on substrate binding revealed by structures of Methylobacterium extorquens malate dehydrogenase. *Acta Crystallogr F Struct Bio lCommun*. 74(10):610-616.

Hadzipasic A, Wilson C, Nguyen V, Kern N, Kim C, Pitsawong W, Villali J, Zheng Y, Kern D. 2020. Ancient origins of allosteric activation in a Ser-Thr kinase. *Science*. 367(6480):912-917.

Halgand F, Houée-Lévin C, Weik M, Madern D. 2020. Remote oxidative modifications induced by oxygen free radicals modify T/R allosteric equilibrium of a hyperthermophilic lactate dehydrogenase. *J Struct Biol*. 210(2):107478.

Hilser VJ, Wrabl JO, Motlagh HN. 2012. Structural and energetic basis of allostery. *Annu Rev Biophys*. 41:585-609.

Holbrook JJ, Liljas A, Steindel SJ, Rossmann MG. 1975. 4 Lactate Dehydrogenase. In: Boyer PD, editor. The Enzymes. Academic Press. p. 191–292.

Huang J, Rauscher S, Nawrocki G, Ran T, Feig M, de Groot BL, et al. 2017. CHARMM36m: an improved force field for folded and intrinsically disordered proteins. *Nat Methods*. 14:71-73.

Huang Z, Mou L, Shen Q, Lu S, Li C, Liu X, Wang G, Li S, Geng L, Liu Y, Wu J, Chen G, Zhang J. 2014. ASD v2.0: updated content and novel features focusing on allosteric regulation. *Nucleic Acids Res*. 42(Database issue):D510-6.

Iacovino LG, Rossi M, Di Stefano G, Rossi V, Binda C, Brigotti M, Tomaselli F, Pasti AP, Dal Piaz F, Cerini S, Hochkoeppler A. 2022. Allosteric transitions of rabbit skeletal muscle lactate dehydrogenase induced by pH-dependent dissociation of the tetrameric enzyme. *Biochimie*. 199:23-35.

Iorio A, Roche J, Engilberge S, Coquelle N, Girard E, Sterpone F, Madern D. 2021. Biochemical, structural and dynamical studies reveal strong differences in the thermal-dependent allosteric behavior of two extremophilic lactate dehydrogenases. *J Struct Biol*. 213(3):107769.

Irimia A, Vellieux FM, Madern D, Zaccaï G, Karshikoff A, Tibbelin G, Ladenstein R, Lien T, Birkeland NK. 2004. The 2.9Å resolution crystal structure of malate dehydrogenase from *Archaeoglobus fulgidus*: mechanisms of oligomerisation and thermal stabilisation. *J Mol Biol*. 335(1):343-356.

Iwata S, Kamata K, Yoshida S, Minowa T, Ohta T. 1994. T and R states in the crystals of bacterial L-lactate dehydrogenase reveal the mechanism for allosteric control. *Nat Struct Biol*. 1(3):176-185.

Johnsen U, Reinhardt A, Landan G, Tria FDK, Turner JM, Davies C, Schönheit P. 2019.New views on an old enzyme: allosteric regulation and evolution of archaeal pyruvate kinases. *FEBS J*. 286(13):2471-2489.

Katava M, Marchi M, Madern D, Sztucki M, Maccarini M, Sterpone F. 2020. Temperature Unmasks Allosteric Propensity in a Thermophilic Malate Dehydrogenase via Dewetting and Collapse. *J Phys Chem B*. 124(6):1001-1008.
Khersonsky O, Tawfik DS. 2010. Enzyme promiscuity: a mechanistic and evolutionary perspective. *Annu Rev Biochem*. 79:471-505.
Kolappan S, Shen DL, Mosi R, Sun J, McEachern EJ, Vocadlo DJ, Craig L. 2015. Structures of lactate dehydrogenase A (LDHA) in apo, ternary and inhibitor-bound forms. *Acta Crystallogr D Biol Crystallogr*. 71(2):185-195.
Koshland DE, Nemethy G, Filmer D. 1966. Comparison of experimental binding data and theoretical models in proteins containing subunits. *Biochemistry*. 5:365-385.
Kuo LC, Zambidis I, Caron C. 1989. Triggering of allostery in an enzyme by a point mutation: ornithine transcarbamoylase. *Science*. 245(4917):522-524.
Langelandsvik AS, Steen IH, Birkeland NK, Lien T. 1997. Properties and primary structure of a thermostable L-malate dehydrogenase from *Archaeoglobusfulgidus. Arch Microbiol*. 168(1):59-67.
Letunic I, Bork P. 2021. Interactive Tree Of Life (iTOL) v5: an online tool for phylogenetic tree display and annotation. *Nucleic Acids Res.* 49(W1):W293-W296.
Lisi GP, Currier AA, Loria JP. 2018. Glutamine Hydrolysis by Imidazole Glycerol Phosphate Synthase Displays Temperature Dependent Allosteric Activation. *Front MolBiosci*. 5:4.
Madern D, Cai XM, Abrahamsen MS, Zhu G. 2004. Evolution of *Cryptosporidium parvum* lactate dehydrogenase from malate dehydrogenase by a very recent event of gene duplication. *MolBiolEvol*21: 489-497.
Madern D, Ebel C, Dale HA, Lien T, Steen IH, Birkeland NK, Zaccai G. 2001. Differences in the oligomeric states of the LDH-like L-MalDH from the hyperthermophilic archaea *Methanococcus jannaschii and Archaeoglobus fulgidus*. *Biochemistry*. 240(34):10310-10316.
Madern D. 2002. Molecular Evolution within the L-Malate and L-Lactate Dehydrogenase Super-Family. *J Mol Evol* 54: 825-840.
Madhu MK, Debroy A, Murarka RK. 2022. Molecular Insights into Phosphorylation-Induced Allosteric Conformational Changes in a β_2-Adrenergic Receptor. *J Phys Chem B.* 126(9):1917-1932.
Makurat S, Cournia Z, Rak J. 2022. Inactive-to-Active Transition of Human Thymidine Kinase 1 Revealed by Molecular Dynamics Simulations. *J Chem Inf Model*. 62(1):142-149.

Mariño Pérez L, Ielasi FS, Bessa LM, Maurin D, Kragelj J, Blackledge M, Salvi N, Bouvignies G, Palencia A, Jensen MR. 2022. Visualizing protein breathing motions associated with aromatic ring flipping. *Nature*. 602(7898):695-700.
Mas-Droux C, Biou V, Dumas R. 2006. Allosteric threonine synthase. Reorganization of the pyridoxal phosphate site upon asymmetric activation through S-adenosyl methionine binding to a novel site. *J Biol Chem*. 281(8):5188-5196.
Matoba Y, Miyasako M, Matsuo K, Oda K, Noda M, Higashikawa F, Kumagai T, Sugiyama M. 2014. An alternative allosteric regulation mechanism of an acidophilic l-lactate dehydrogenase from *Enterococcus mundtii* 15-1A. *FEBS Open Bio*. 4:834-847.
McClendon S, Zhadin N, Callender R. 2005. The approach to the Michaelis complex in lactate dehydrogenase: the substrate binding pathway. *Biophys J*. 89(3):2024-2032.
Minárik P, Tomásková N, Kollárová M, Antalík M. 2002. Malate dehydrogenases--structure and function. *Gen Physiol Biophys*. 21(3):257-265.
Modi T, Campitelli P, Kazan IC, Ozkan SB. 2021. Protein folding stability and binding interactions through the lens of evolution: a dynamical perspective. *Curr Opin Struct Biol*. 66:207-215.
Monod J, Wyman J, Changeux JP. 1965. On the nature of allosteric transitions, a plausible model. *J Mol Biol*. 12: 88-118.
Motlagh HN, Wrabl JO, Li J, Hilser VJ. 2014. The ensemble nature of allostery. *Nature*. 508(7496):331-339.
Okafor CD, Hercules D, Kell SA, Ortlund EA. 2020. Rewiring Ancient Residue Interaction Networks Drove the Evolution of Specificity in Steroid Receptors. *Structure*. 28(2):196-205.e3.
Otten R, Liu L, Kenner LR, Clarkson MW, Mavor D, Tawfik DS, Kern D, Fraser JS. 2018. Rescue of conformational dynamics in enzyme catalysis by directed evolution. *Nat Commun*. 9(1):1314.
Piontek K, Chakrabarti P, Schär HP, Rossmann MG, Zuber H. 1990. Structure determination and refinement of *Bacillus stearothermophilus* lactate dehydrogenase. *Proteins*. 7(1):74-92.
Poelwijk FJ, Krishna V, Ranganathan R. 2016. The Context-Dependence of Mutations: A Linkage of Formalisms. *PLoS Comput Biol*. 12(6):e1004771.
Raman AS, White KI, Ranganathan R. 2016. Origins of Allostery and Evolvability in Proteins: A Case Study. *Cell*. 166(2):468-480.
Reynolds KA, McLaughlin RN, Ranganathan R. 2011. Hot spots for allosteric regulation on protein surfaces. *Cell*. 147(7):1564-1575.

Roche J, Girard E, Mas C, Madern D. 2019. The archaeal LDH-like malate dehydrogenase from *Ignicoccus islandicus* displays dual substrate recognition, hidden allostery and a non-canonical tetrameric oligomeric organization. *J Struct Biol*. 208(1):7-17.
Rodicio R, Strauss A, Heinisch JJ. 2000. Single point mutations in either gene encoding the subunits of the hetero octameric yeast phosphofructokinase abolish allosteric inhibition by ATP. *J Biol Chem*. 275(52):40952-40960.
Sakowicz R, Kallwass HK, Parris W, Kay CM, Jones JB, Gold M. 1993. Threonine 246 at the active site of the L-lactate dehydrogenase of *Bacillus stearothermophilus* is important for catalysis but not for substrate binding. *Biochemistry*. 32(47):12730-12735.
Schrank TP, Bolen DW, Hilser VJ. 2009. Rational modulation of conformational fluctuations in adenylate kinase reveals a local unfolding mechanism for allostery and functional adaptation in proteins. *Proc Natl Acad Sci U S A*. 106(40):16984-16989.
Schroeder G, Matsuzawa H, Ohta T. 1988. Involvement of the conserved histidine-188 residue in the L-lactate dehydrogenase from *Thermus caldophilus* GK24 in allosteric regulation by fructose 1,6-bisphosphate. *Biochem Biophys Res Commun*.152 (3):1236-1241.
Schupfner M, Straub K, Busch F, Merkl R, Sterner R. 2020. Analysis of allosteric communication in a multi enzyme complex by ancestral sequence reconstruction. *Proc Natl AcadSci U S A*. 117(1):346-354.
Stebbins JW, Kantrowitz ER. 1992. Conversion of the non-cooperative *Bacillus subtilis* aspartate transcarbamoylase into a cooperative enzyme by a single amino acid substitution. Biochemistry. 31(8):2328-2332.
Steindel PA, Chen EH, Wirth JD, Theobald DL. 2016. Gradual neofunctionalization in the convergent evolution of trichomonad lactate and malate dehydrogenases. *Protein Sci*. 25(7):1319-1331.
Suplatov D, Švedas V. 2015. Study of Functional and Allosteric Sites in Protein Super families. *Acta Naturae*. 7(4):34-45.
Taguchi H. 2017. The Simple and Unique Allosteric Machinery of *Thermus caldophilus* Lactate Dehydrogenase: Structure-Function Relationship in Bacterial Allosteric LDHs. *Adv Exp Med Biol*. 925:117-145.
Thornton JW, Need E, Crews D. 2003. Resurrecting the Ancestral Steroid Receptor: Ancient Origin of Estrogen Signaling. *Science*. 301(5640): 1714-1717.
Tokuriki N, Tawfik DS. 2009. Protein dynamism and evolvability. *Science*.324(5924):203-207.

Uchikoba H, Fushinobu S, Wakagi T, Konno M, Taguchi H, Matsuzawa H. 2002. Crystal structure of non-allosteric L-lactate dehydrogenase from *Lactobacillus pentosus* at 2.3 Å resolution: specific interactions at subunit interfaces. *Proteins*. 46(2):206-214.
Van Der Spoel D, Lindahl E, Hess B, Groenhof G, Mark AE, Berendsen HJ. 2005. GROMACS: fast, flexible, and free. *J Comput Chem.* 26:1701-1718.
Vogel M, Bukau B, Mayer MP. 2006. Allosteric regulation of Hsp70 chaperones by a proline switch. *Mol Cell*. 21(3):359-367.
Waterhouse A, Bertoni M, Bienert S, Studer G, Tauriello G, Gumienny R, Heer FT, de Beer TAP, Rempfer C, Bordoli L, Lepore R, Schwede T. 2018. SWISS-MODEL: homology modelling of protein structures and complexes. *Nucleic Acids Res*. 46(W1):W296-W303.
Wei S, Roessler BC, Chauvet S, Guo J, Hartman JL 4th, Kirk KL. 2014. Conserved allosteric hot spots in the transmembrane domains of cystic fibrosis transmembrane conductance regulator (CFTR) channels and multidrug resistance protein (MRP) pumps. *J Biol Chem*. 289(29):19942-19957.
Weyand M, Schlichting I, Herde P, Marabotti A, Mozzarelli A. 2002. Crystal structure of the beta Ser178--> Pro mutant of tryptophan synthase. A "knock-out" allosteric enzyme. *J Biol Chem.* 277(12):10653-10660.
Wigley DB, Gamblin SJ, Turkenburg JP, Dodson EJ, Piontek K, Muirhead H, Holbrook JJ. 1992. Structure of a ternary complex of an allosteric lactate dehydrogenase from *Bacillus stearothermophilus* at 2.5 Å resolution. *J Mol Biol*. 223(1):317-335.
Wilks HM, Hart KW, Feeney R, Dunn CR, Muirhead H, Chia WN, Barstow DA, Atkinson T, Clarke AR, Holbrook JJ. 1988. A specific, highly active malate dehydrogenase by redesign of a lactate dehydrogenase framework. *Science*. 242(4885):1541-1544.
Winter VJ, Cameron A, Tranter R, Sessions RB, Brady RL. 2003. Crystal structure of *Plasmodium berghei* lactate dehydrogenase indicates the unique structural differences of these enzymes are shared across the Plasmodium genus. *Mol Biochem Parasitol*. 131(1):1-10.
Wodak SJ, Paci E, Dokholyan NV, Berezovsky IN, Horovitz A, Li J, et al. 2019 Allostery in Its Many Disguises: From Theory to Applications. *Structure*. 27:566-78.
Wouters MA, Liu K, Riek P, Husain A. 2003. A despecialization step underlying evolution of a family of serine proteases. *Mol Cell*. 12(2):343-354.
Wrabl JO, Gu J, Liu T, Schrank TP, Whitten ST, Hilser VJ. 2011. The role of protein conformational fluctuations in allostery, function, and evolution. *Biophys Chem*. 159(1):129-141.

Yin Y, Kirsch JF. 2007. Identification of functional paralog shift mutations: conversion of Escherichia coli malate dehydrogenase to a lactate dehydrogenase. *Proc Natl Acad Sci U S A.* 104(44):17353-17357

Zhou Y, Zhou H, Karplus M. 20023. Cooperativity in Scapharca dimeric hemoglobin: simulation of binding intermediates and elucidation of the role of interfacial water. *J Mol Biol*. 326(2):593-606.

Zou T, Risso VA, Gavira JA, Sanchez-Ruiz JM, Ozkan SB. 2015. Evolution of conformational dynamics determines the conversion of a promiscuous generalist into a specialist enzyme. *Mol Biol Evol*. 32(1):132-143.

Wolf S, Sohmen B, Hellenkamp B, Thurn J, Stock G, Hugel T. 2021. Hierarchical dynamics in allostery following ATP hydrolysis monitored by single molecule FRET measurements and MD simulations. *Chem Sci*. 12(9):3350-3359.